Ectopic Expression of a Maize Gene Is Induced by Composite Insertions Generated Through Alternative Transposition

Weijia Su,* Tao Zuo,* and Thomas Peterson*,†,1

*Department of Genetics, Development, and Cell Biology and †Department of Agronomy, Iowa State University, Ames, Iowa 50011-3260

ORCID IDs: 0000-0001-9903-761X (W.S.); 0000-0002-6581-1192 (T.Z.); 0000-0002-9933-7556 (T.P.)

ABSTRACT Transposable elements (TEs) are DNA sequences that can mobilize and proliferate throughout eukaryotic genomes. Previous studies have shown that in plant genomes, TEs can influence gene expression in various ways, such as inserting in introns or exons to alter transcript structure and content, and providing novel promoters and regulatory elements to generate new regulatory patterns. Furthermore, TEs can also regulate gene expression at the epigenetic level by modifying chromatin structure, changing DNA methylation status, and generating small RNAs. In this study, we demonstrated that *Ac*/fractured *Ac (fAc)* TEs are able to induce ectopic gene expression by duplicating and shuffling enhancer elements. *Ac/fAc* elements belong to the *hAT* family of class II TEs. They can undergo standard transposition events, which involve the two termini of a single transposon, or alternative transposition events that involve the termini of two different nearby elements. Our previous studies have shown that alternative transposition can generate various genome rearrangements such as deletions, duplications, inversions, translocations, and composite insertions (CIs). We identified >50 independent cases of CIs generated by *Ac/fAc* alternative transposition and analyzed 10 of them in detail. We show that these CIs induced ectopic expression of the maize *pericarp color 2* (*p2*) gene, which encodes a Myb-related protein. All the CIs analyzed contain sequences including a transcriptional enhancer derived from the nearby *p1* gene, suggesting that the CI-induced activation of *p2* is affected by mobilization of the *p1* enhancer. This is further supported by analysis of a mutant in which the CI is excised and *p2* expression is lost. These results show that alternative transposition events are not only able to induce genome rearrangements, but also generate CIs that can control gene expression.

KEYWORDS transposable elements; alternative transposition; composite insertion; enhancer

Transposable Elements (TEs) are DNA sequences that can move their positions and proliferate themselves in the genomes. Wicker *et al.* published a unified classification system for TEs in 2007 (Wicker *et al.* 2007). There are two types of TE: class I TEs are also called RNA elements, since their transpositions rely on RNA as intermediates; class II TEs do not need RNA for their transpositions, therefore they are also called DNA elements. Class II TEs can undergo standard transpositions: TE-encoded transposase binds to the termini of a single TE and facilitates the excision and insertion of the TE. In contrast, at least some class II TEs can also undergo alternative transpositions, which involve the termini of two TEs. This mechanism has been observed in various species and is mediated by different TE families (Gray 2000), including IS*10*/Tn*10* in bacteria (Chalmers and Kleckner 1996), Tam*3* in snapdragon (Martin and Lister 1989), *P* elements in *Drosophila* (Gray *et al.* 1996), and *Ac/Ds* elements in maize (Weil and Wessler 1993). In this study, we focused on characterizing the products of a specific type of alternative transposition reaction driven by maize *Ac/Ds* elements. *Ac/Ds* was the first TE system discovered by Barbara McClintock in the 1940s (McClintock 1947, 1950). *Ac* is the autonomous element, which encodes the transposase enzyme, and *Ds* is the nonautonomous counterpart that requires *Ac* transposase for transposition. Previous work in maize has shown that *Ac/Ds* can undergo two major types of alternative transposition:

doi: https://doi.org/10.1534/genetics.120.303592
Manuscript received August 9, 2020; accepted for publication September 23, 2020; published Early Online September 28, 2020.
Available freely online through the author-supported open access option.
Supplemental material available at figshare: https://doi.org/10.25386/genetics.13010303.
[1]Corresponding author: Molecular Biology Bldg. #2258, Iowa State University, 2437 Pammel Dr, Ames, IA 50011-3260. E-mail: thomasp@iastate.edu

reversed ends transposition (RET) involves the reversely oriented termini of two different elements on the same chromosome, while sister chromatid transposition (SCT) targets the termini of two TEs located on different sister chromatids (Huang and Dooner 2008; Peterson and Zhang 2013). Previous studies have shown that SCT can generate deletions, inverted duplications (Zhang and Peterson 1999, 2005), sister chromatid fusions, and chromosome breaks (Yu *et al.* 2010); while RET can generate deletions (Zhang and Peterson 2005), direct duplications (Zhang *et al.* 2013), inversions, and translocations (Zhang and Peterson 1999, 2004; Zhang *et al.* 2009). In addition, both SCT and RET can generate novel compound structures termed composite insertions (CIs) (Zhang *et al.* 2014; Wang *et al.* 2020).

In addition to generating genome rearrangements, TEs can affect gene expression in many different ways (Hirsch and Springer 2017). For example, TE insertion in introns can alter splicing patterns, leading to new transcripts and protein products (Luehrsen and Walbot 1990). Many studies have shown that TEs can provide novel promoters to drive expression of adjacent genes (Butelli *et al.* 2012). In certain conditions, TEs may provide enhancer sequences that trigger stress-induced gene expression (Makarevitch *et al.* 2015). Additionally, TEs may exert epigenetic effects on nearby genes, such as inducing the spread of DNA methylation from TEs to flanking sequences, thereby suppressing expression of neighboring genes (Hollister and Gaut 2009). Moreover, TEs may alter chromatin states and thereby influence gene expression: Eichten *et al.* (2012) reported increased heterochromatin and reduced gene expression in the vicinity of TE insertions.

Enhancers are important *cis*-regulatory elements in eukaryotic genomes. Enhancers are typically short (50–1500 bp) and bound by transcription factors to activate gene expression (Blackwood and Kadonaga 1998). They can be located upstream or downstream of the target genes, and they may function over long distances by forming chromatin loops (Krivega and Dean 2012). In maize, only a small number of enhancers have been identified and characterized (Oka *et al.* 2017). For example, the enhancer of the maize *booster1* (*b1*) gene consists of multiple tandem 853-bp repeats located ~100 kb upstream of the *b1* coding sequence (Stam *et al.* 2002). The enhancer of *teosinte branched 1* (*tb1*), a maize domestication gene (Doebley *et al.* 1995), is located ~60 kb upstream of the *tb1* target gene (Clark *et al.* 2006). The gene *pericarp color1* (*p1*) controls biosynthesis of a red phlobaphene pigment in multiple maize organs such as pericarp, cob, and silk. *p1* expression is regulated by dual enhancer sequences that are repeated at sites upstream and downstream of the *p1* coding sequence. Fragment 15 (*f15*) is located downstream of the *p1* coding region (Lechelt *et al.* 1989) and acts as a floral organ enhancer (Sidorenko *et al.* 1999). In this study, we show that *p1* enhancer *f15* can be mobilized by alternative transposition events to activate ectopic expression of a second maize gene. These results demonstrate the potential impacts of terminal inverted repeat (TIR) TEs and alternative transposition events on maize genome evolution.

Materials and Methods

Maize genetic stocks and screen

The progenitor allele *p1-wwB54* has *p1* loss-of-function due to the deletion of the first two exons of *p1*, therefore, it yields white pericarps and white cobs. To screen for new RET events resulting in *pericarp color 2* (*p2*) expression, ~4000 plants of genotype *p1-wwB54* heterozygous with a *p1* null allele (*p1-ww [4Co63]*) were grown in an isolation field and allowed to pollinate with *p1-ww[4Co63]* pollen parents. The resulting ears were screened, and kernels with red pericarps were selected and propagated. The potential heritability of each red sector is roughly proportional to the area of kernels covered by that sector (Emerson 1917). Moreover, one-half of all new potentially heritable mutations will not be recovered due to segregation in the female meiosis. From ~4000 *p1-wwB54/p1-ww* ears, we identified ~400 half-kernel red sectors, ~40 whole-kernel events, and several multi-kernel sectors and whole-ear events (Figure 3). Following propagation of these cases, we obtained ~50 heritable new alleles with red kernel pericarps that were further analyzed for insertions in *p2* (Supplemental Material, File S1). Genomic DNA (gDNA) samples were screened by PCR using primers located in *Ac* and fractured *Ac* (*fAc*), paired with primers from the *p2* gene sequence. Samples giving positive results for both *5′Ac/p2* and *3′fAc/p2* junctions were considered to be candidate CI alleles. The candidate CI alleles were then planted and self-pollinated to generate homozygotes for analysis. To screen for further mutations of CI *S7* and *E3* alleles, plants carrying these alleles were self-pollinated or crossed with *p1-ww [4Co63]* in the isolation field; in resulting ears, kernels with white (*S7M*) or light red pericarps (*E3M*) were selected as mutants derived from the respective CIs.

DNA extraction and PCR

Total gDNA was prepared by using a modified cetyltrimethylammonium bromide extraction protocol from leaves of 3-week-old plants. Promega (Madison, WI) GoTaq Green Master Mix was used for PCR reactions. The PCR was initiated by a 2-min denaturation at 95°, then 30 sec of annealing step at a temperature of 5° below the melting temperature of the primers, then 1 min extension per kb at 72°; these steps were repeated for 30 cycles and a final extension at 72° for 5 min was applied.

RT-PCR

Total RNA was extracted by Invitrogen (Carlsbad, CA) TRIzol Reagent from maize pericarp 20 days after pollination and treated with New England Biolabs (Beverly, MA) DNase I to remove gDNA. Complementary DNA (cDNA) was prepared by Invitrogen SuperScript II Reverse Transcriptase kit and used as the RT-PCR template.

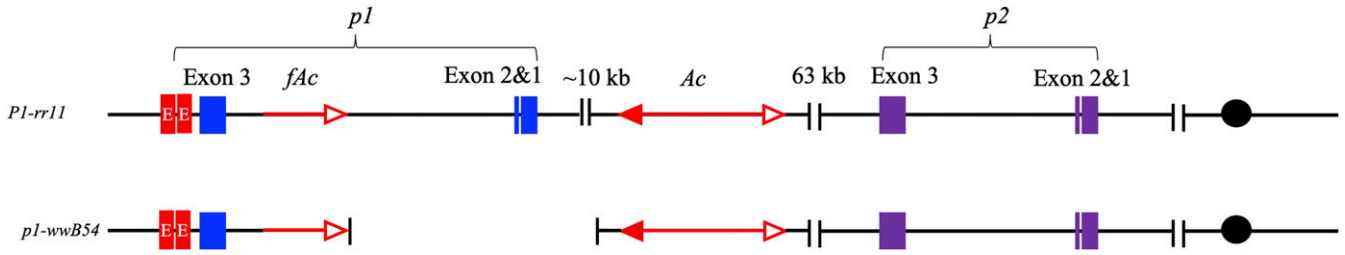

Figure 1 Structures of *P1-rr11* and *p1-wwB54*. The upper line indicates the structure of the progenitor allele *P1-rr11*. The lower line indicates the structure of *B54*, which has a deletion of exon 1 and exon 2 of *p1*. The blue and purple boxes indicate the exons of the *p1* and *p2* genes, respectively; red boxes indicate copies of enhancer *f15*. The arrow with a single open arrowhead indicates fractured *Ac* (*fAc*); double-headed arrow indicates full-length *Ac* element. Black dots indicate the centromere of chromosome 1.

Bisulfite sequencing

Bisulfite treatment was performed using the EZ DNA Methylation-Lightning Kit from Zymo Research. The bisulfite-converted DNA was used as template for PCR using primers that were designed based on the converted sequences. Sequence conversion was done using the program MethPrimer2.0 (http://www.urogene.org/methprimer2/tester-invitation.html) (Li and Dahiya 2002).

Data availability

Maize genetic stocks are available by request to T.P. Sequences reported here are available in the Supplemental Material. The sequence of *p1-wwB54* and flanking regions compiled from previous sequence files and CI sequences (this report) is available at GenBank (accession number: MW008479). Supplemental material available at figshare: https://doi.org/10.25386/genetics.13010303.

Results

CIs produced from B54 via RET during DNA replication

The *p1* gene encodes an R2R3 Myb transcriptional factor (Grotewold *et al.* 1991), and regulates phlobaphene biosynthesis in maize floral organs including kernel pericarp and cob glumes (Dooner *et al.* 1991). *p2* is a paralog of *p1*, but is not expressed in pericarp and cob. Both *p1* and *p2* are located on the short arm of maize chromosome 1, separated by ~70 kb (Zhang *et al.* 2000). Phenotypes of *p1* alleles are commonly identified by a two-letter suffix that indicates the color of kernel pericarp and cob. For example, *p1-ww* indicates white pericarp and white cob, and *p1-wr* indicates white pericarp and red cob (Anderson 1924). The *P1-rr11* allele conditions red pigmentation of kernel pericarp and cob. It contains an intact *p1* gene with a full-length (4565 bp) *Ac* element inserted upstream of *p1* exon 1, and an *fAc* (only 2039 bp 3′ of *Ac*) inserted in *p1* intron 2 (Figure 1) (Zhang and Peterson 2004). In a previous study, Yu *et al.* (2011) showed that the *Ac* and *fAc* termini in *P1-rr11* could undergo RET to induce deletions of the DNA between the *Ac/fAc* termini. In one case, deletion of *p1* exons 1 and 2 produced a mutant allele termed *p1-wwB54* (hereafter referred to as *B54)* with colorless pericarp and cob. The *B54* allele retains the *Ac* and *fAc* elements in reversed orientation, with the 5′ terminus of *Ac* and 3′ terminus of *fAc* separated by a segment of 331 bp (Figure 1). In this configuration, the *Ac* and *fAc* termini in *B54* can generate sister chromatid fusions and chromosome breaks (Yu *et al.* 2011).

Using a different *p1* allele, a previous study showed that a pair of reverse-oriented *Ac/fAc* in *p1* can undergo RET and induce DNA rereplication to generate flanking duplications and novel structures termed CIs (Zhang 2013, 2014) (because the formation of duplications was previously described in detail, here we focus on the formation and action of the CIs). We hypothesized that *p1-wwB54* may also produce CIs via RET during DNA replication, as shown in Figure 2. In this model, the *Ac* transposase excises the 3′ end of *fAc* and 5′ end of *Ac* from a region of replicated DNA, and inserts these termini into an unreplicated target site. This insertion generates a rolling circle replicon to rereplicate *Ac* and flanking sequences, while *fAc* and its flanking sequence will be rereplicated by elongation of the impinging replicon. At some point, rereplication spontaneously aborts to produce two broken ends with double-strand breaks (DSBs). The fusion of these two DSBs will rejoin the two chromosome fragments and generate a CI at the new junction (Zhang *et al.* 2014). If the rereplication fork through *fAc* is sufficiently extended, the CI is expected to include a copy of *p1* exon 3 and transcriptional enhancer element *f15*.

Unexpected reversion of deletion allele p1-wwB54

Initial observations of maize ears produced by plants containing *p1-wwB54* showed that many kernels contained red sectors resembling the red revertant sectors typical of somatic reversion of *p1-vv* to *P1-rr* (Emerson 1929). This was surprising, considering that both exons 1 and 2 of the *p1* gene were deleted in *p1-wwB54*. These two exons contain most of the coding sequence for the Myb DNA-binding domain that is essential for *p1* function (Grotewold *et al.* 1991). We hypothesized that these sectors may result from ectopic expression of the *p2* gene, a *p1* paralog located ~70 kb proximal to *p1* (Zhang *et al.* 2000). The *p1* and *p2* genes encode highly similar (95% identical) proteins (Zhang *et al.* 2000), and previous studies have shown that *p2/p1* chimeric genes are capable of producing pericarp pigment (Zhang *et al.* 2006;

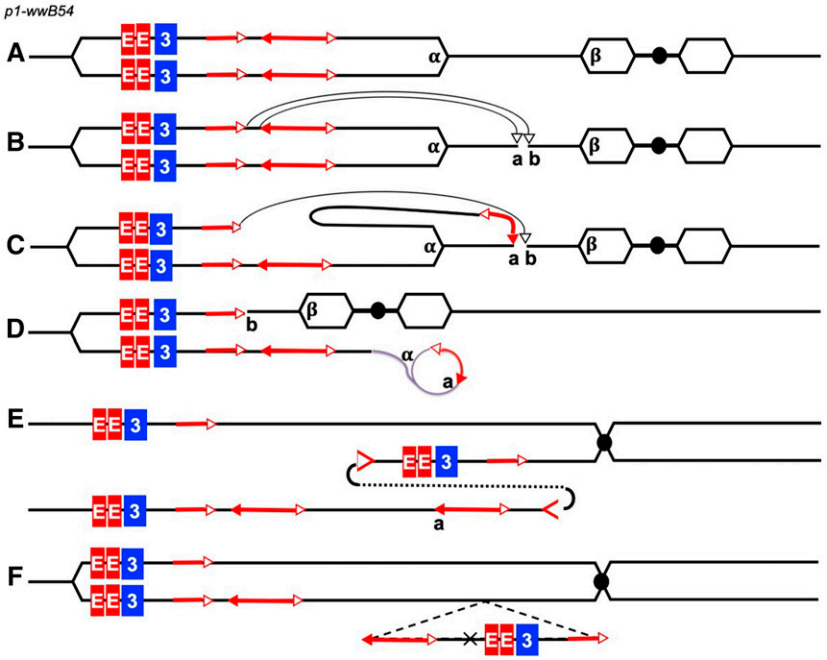

Figure 2 Model of CI formation from *p1-wwB54*. (A) The structure of the allele *p1-wwB54*. The hexagons indicate replicons. α and β indicate two replication forks. Other symbols have the same meaning as in Figure 1. (B) Transposase binds to the *fAc* and *Ac* and the two termini insert into the target site *a*/*b*, which is not yet replicated. (C) The insertion of *Ac* generates a rolling circle replicon and the insertion of *fAc* joins with target site b. (D) *Ac* and its flanking sequence are rereplicated by the rolling circle replicon. (E) The rereplication aborts and the two double-strand breaks (indicated by > and <) fuse together. (F) A CI is generated containing *Ac*, *fAc*, *p1* exon 3, and enhancer *f15*, and a portion of the flanking sequences. CI, composite insertion; *fAc*, fractured *Ac*.

Wang *et al.* 2015). Therefore, we hypothesized that the red sectors observed on *p1-wwB54* ears represented activation of *p2* expression, possibly by CIs carrying and inserting a copy of the *p1* enhancer element in or near *p2*. The insertion of the *p1* enhancer would induce ectopic expression of *p2*, resulting in the red pericarp sectors observed on *p1-wwB54* ears. To test this hypothesis, we screened ears produced from plants carrying *p1-wwB54* and selected kernels with red pericarp sectors ranging in size from around one-half of a kernel to the whole ear (Figure 3 and File S1). Because the maize kernel pericarp is derived from the ovary wall that gives rise to the female gametophyte, premeiotic mutations in the developing ear tissues can produce clonal sectors that are expressed in the pericarp and also inherited by the kernel embryo (Emerson 1917). However, due to the intervening meiosis, each new mutant allele has only a 50% chance of being transmitted to the embryo. About 450 kernels from independent red sectors (*Materials and Methods*) were grown and propagated to establish a new allelic series of 50 orange and red pericarp types derived from the *p1-wwB54* allele (File S1).

Identification of CIs at the p2 locus

The 50 new revertant alleles obtained from the screen described above were analyzed for structural changes in the *p2* gene. First, using genomic PCR and Southern blot analysis (not shown), we determined that a large majority of alleles tested do indeed carry new CIs inserted in or near the *p2* gene. For 24 cases, we mapped the sites of CI insertion by PCR using primers specific for *Ac* or *fAc* sequences, paired with primers in *p2* (File S2). Reversed primers in *Ac* (*Ac-r*) were paired with reversed primers in *p2* (*p2-r*) to amplify the *Ac* junction, followed by a second PCR using *p2-f* plus *fAc-f* primers to amplify the *fAc* junction (Figure 4A and File S3). Figure 4B shows the PCR results from 10 CI alleles as examples. PCR products were sequenced and compared with *p2* genomic sequence to identify the precise insertion sites in 24 CI alleles: 10 cases contained CIs in the *p2* promoter region, while 14 cases had CIs in *p2* intron 2. Among these 24 CIs, 21 of them had the same orientation as shown in

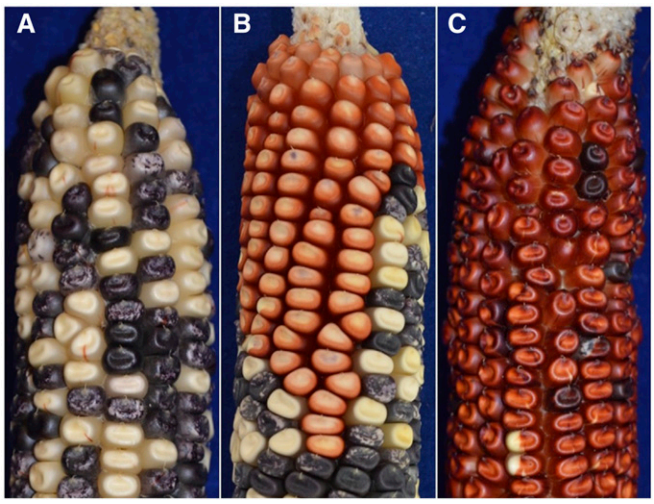

Figure 3 Screening for new CI alleles derived from *p1-wwB54*. (A) Maize ear with typical *p1-wwB54* phenotype with predominantly colorless pericarp, and small, infrequent red revertant sectors. (B) Ear grown from *p1-wwB54* kernel, with a large multikernel red sector (upper) on an ear with otherwise typical *p1-wwB54* phenotype (lower portion of ear). (C) Ear grown from *p1-wwB54* kernel with whole-ear red pericarp. Infrequent colorless sectors suggest ongoing instability of this novel allele, most likely due to *Ac* activity. In all ears, solid-colored and spotted kernels reflect *Ac*-induced excision of *Ds* element from *r1-m3::Ds* allele, resulting in sectors of purple kernel aleurone. CI, composite insertion.

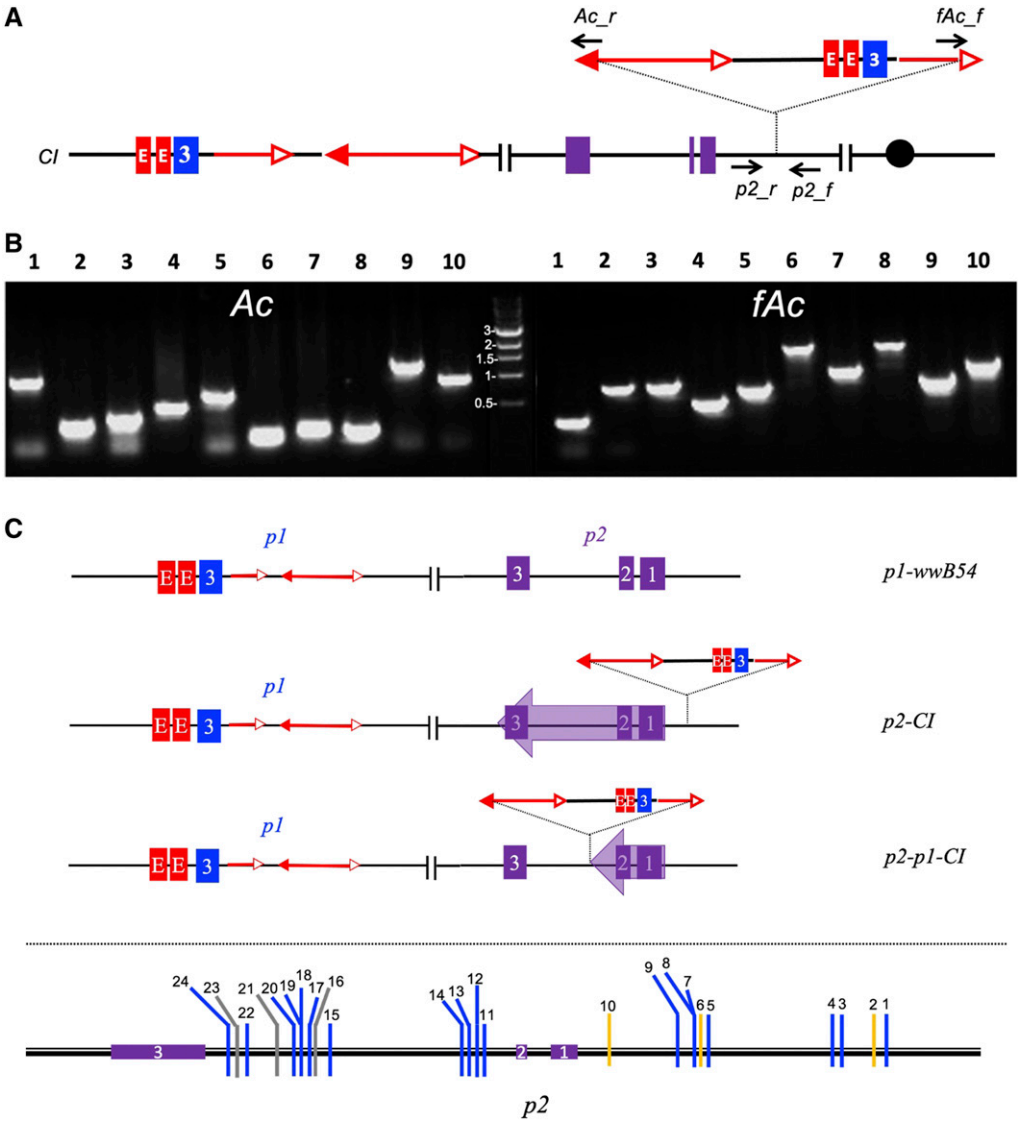

Figure 4 Identification of CI insertion sites. (A) The primer sets used for detection of CI target sites. *Ac_r* indicates a set of primers located on *Ac* 5′ end in a reversed orientation, *fAc_f* indicates primers located on *fAc* 3′ end in a forward orientation. *p2_r* and *p2_f* indicate primers in flanking *p2* sequence. (B) Results showing PCR amplification of *Ac* and *fAc* junction fragments from 10 independent CI alleles. Note that fragment sizes will vary depending on insertion site and flanking *p2* primers. Central lane is DNA size marker. (C) Map of CI insertions in *p2*. Upper panel: diagrams of structures of progenitor *p1-wwB54* and two types of *CI* alleles: *p2-CI* has CI insertion in *p2* promoter region and *p2/p1-CI* has CI insertion into *p2* intron 2. CI insertions upstream of *p2* can induce transcription of the intact *p2* gene; while CI insertion into *p2* intron 2 can generate a chimeric *p2/p1* gene (Zhang and Peterson 2005; Wang *et al.* 2015). Lower panel: positions and orientations of 24 CIs in *p2*. In 10 cases, CIs are inserted in the *p2* promoter region (1–10), while 14 cases (11–24) have CIs inserted in *p2* intron 2. Blue lines indicate 18 insertions in the common orientation shown in (A); orange lines indicate 3 insertions in the opposite orientation; and 3 gray lines indicate three cases in common orientation in which the *Ac* element has excised. CI, composite insertion; *fAc*, fractured *Ac*.

Figure 4A, with the *Ac* 5′ end closest to *p2* exon 3; and 3 cases had the opposite orientation, in which the *fAc* 3′ end was closest to *p2* exon 3 (Figure 4C). By comparing the sequences of the *Ac* and *fAc* junctions in *p2*, we determined that each CI is flanked by an 8-bp target site duplication (TSD), which is a characteristic feature of *Ac/Ds* insertion (File S2). This finding confirms that the CIs are indeed generated by an *Ac/fAc* transposition event, consistent with the model proposed in Figure 2. Finally, we also identified three alleles in which the *Ac* element had excised from the CI, leaving behind a partial CI containing *fAc* and the *p1* sequences including the enhancer *f15*. This indicates that following CI formation, the *Ac* TE is still active and capable of subsequent independent transposition (Figure 4C and File S2).

According to the model shown in Figure 2, DNA rereplication resulting from alternative transposition should generate CIs with varying sizes and sequence compositions. However, all CIs should contain sequences flanking the original *Ac* donor site, with *p1* 5′ sequences (upstream of *Ac*) fused to *p1* 3′ sequences (downstream of *fAc*) as shown in Figure 5A. Moreover, *p1* forward and *p1* reverse PCR primers, which are divergent in *p1-wwB54*, should converge in each CI across the internal junction. To test this, we analyzed the internal structures of 10 independent CIs. The internal junction products were amplified by combinations of primers including *p1-r* + *p1-f* as shown in Figure 5A, and *Ac-f* + *p1-f* for those cases in which the internal junction was sufficiently close to the *Ac* 3′ end (File S4). Due to the heterogeneity of CI length and structure, PCR was performed using a series of *p1* forward and reverse primers to scan the region. In this way, we isolated and sequenced the internal junctions of 10 independent CIs (Figure 5B and File S5); based on the internal junction sequences, we could surmise the structure of each case (Figure 5C). The 10 CIs range in size from 12.8 to 23.6 kb, including the *Ac* and *fAc* elements flanking each CI. In 6 out of the 10 alleles analyzed, the internal junctions contained microhomologies of

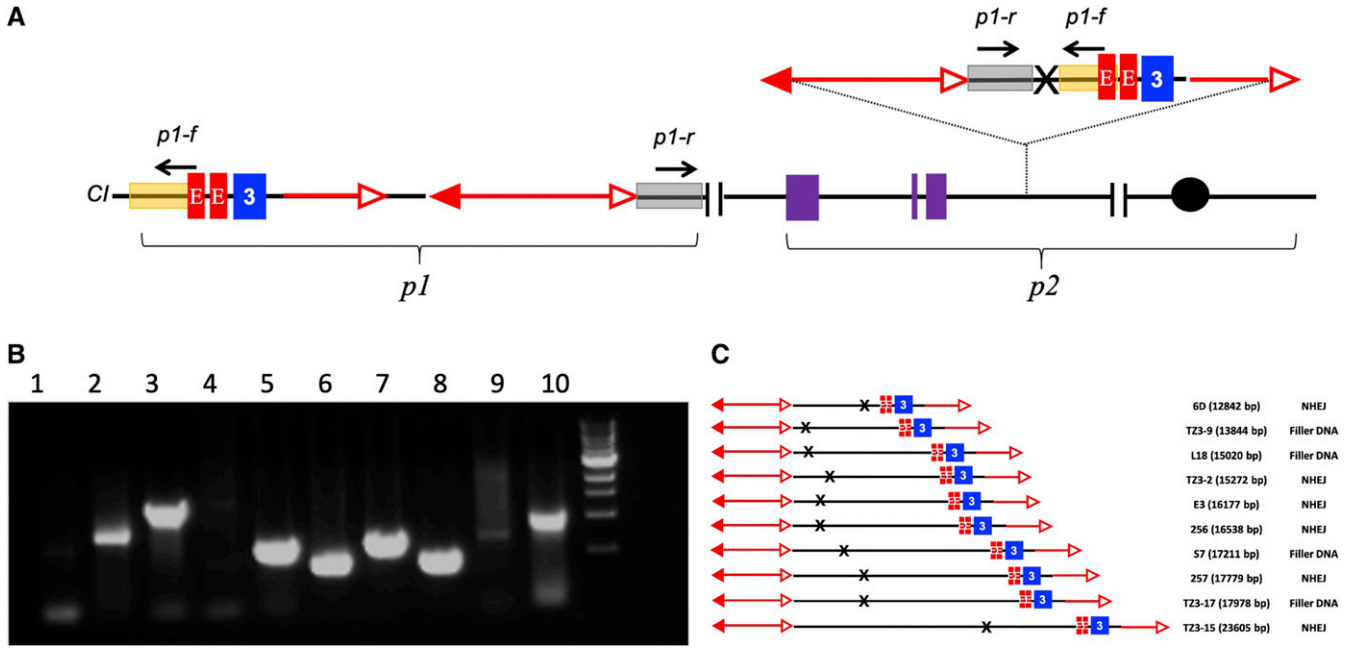

Figure 5 Identification of CI internal structures. (A) Structure of representative chromosome containing the original *p1-wwB54* structure and a new CI insertion into the *p2* 5′ region. *p1-r* and *p1-f* represent sets of forward and reverse primers that are divergent in *p1-wwB54* (left), but convergent in CI (right). (B) Results of PCR to amplify internal junctions of 10 CIs using *p1-f* and *p1-r* primers shown in (A). The samples tested here correspond to the same 10 CI examples shown in Figure 4B. Bands vary in intensity due to different PCR efficiencies using primers specific for each CI junction. (C) CI structures in 10 representative alleles; the first column indicates CI names, with CI sizes in parenthesis; the second column indicates the DSB repair mechanism inferred from the junction sequences. CI, composite insertion; DBS, double-strand break.

3–19 bp, which are consistent with DSB repair via nonhomologous end joining (NHEJ) or microhomology-mediated end joining (Moore and Haber 1996; McVey and Lee 2008). The remaining four CI alleles contain additional filler DNA sequences inserted at each junction. These filler DNA sequences ranged in size from 4 to 50 bp and were apparently copied from nearby (within 100 bp) *p1* sequences, consistent with a template-switch mechanism as reported in previous studies (Wessler *et al.* 1990) (File S5). Based on the internal CI sequences, we compiled an extended *p1* genomic sequence file comprising 14.8 kb upstream and 14.2 kb downstream of the *p1* coding region (MW008479).

Evidence that CI insertion drives p2 expression

Importantly, all of the 10 CI cases examined in detail contain 3′ *p1* sequences, including transcriptional enhancer fragment 15 (indicated as red "E" box in Figure 5). This is consistent with the hypothesis that ectopic expression of *p2* in kernel pericarp in the CI-containing alleles is driven by the *p1* enhancer. A corollary to this hypothesis is that excision of the CI should result in loss of *p2* expression and reversion to the progenitor *p1-wwB54* phenotype. Excision of the CI as a macrotransposon may be expected, considering that it contains suitably oriented *Ac* and *fAc* transposons at each end (Huang and Dooner 2008). Indeed, many of the CI alleles exhibited variably sized sectors of colorless and or less-pigmented pericarp (*e.g.*, Figure 3C).

To test this hypothesis, we examined ears produced by *p2-S7*, an allele containing a 17.2 kb CI inserted upstream of *p2*. As shown in Figure 6, *p2-S7* conditions red kernel pericarp with some colorless sectors. Among ~50 ears grown from *p2-S7* progenies, we identified one ear that had a large clonal sector of ~20 kernels with near-colorless pericarp. Kernels from this sector gave rise to the stable mutant called *p2-S7M*, which has a phenotype of colorless pericarp with some red sectors, similar to the *p1-wwB54* allele (Figure 6A). We analyzed the structure of *p2-S7M* by PCR using primers to amplify the original CI insertion site in *p2*, both *Ac* and *fAc* junctions with *p2*, and the internal CI junction (Figure 6B). The results (Figure 6, B and C) show that in *p2-S7M*, the CI excised from the target site as a macrotransposon, leaving behind the 8-bp TSD from the original insertion. These results show that *p2* expression was indeed a result of CI insertion, and that removal of the CI eliminates the expression of *p2* and restores the phenotype of the progenitor *B54* allele.

To further test *p2* expression in the CI alleles, we measured *p2* transcript levels in *p1-wwB54*, *p2-S7*, and *p2-S7M* by RT-PCR (Figure 6D). Total RNA was prepared from developing kernel pericarp, reverse-transcribed into cDNA, and amplified with PCR primers located in *p2* exons 1 and 2 (*p2-e1* and *p2-e2* in Figure 6B and File S6). Primers complementary to the GPD gene were included as an internal control. The RT-PCR results showed that *p2* transcripts were detected only in the CI allele *p2-S7*, and were undetectable in progenitor *p1-wwB54* and descendent *p2-S7M* in which the CI had excised. PCR products were sequenced to confirm their origin from the *p2* gene (File S7). These results confirm that the red pericarp phenotype was caused by the expression of *p2*, and that *p2* expression is dependent on the presence of a CI.

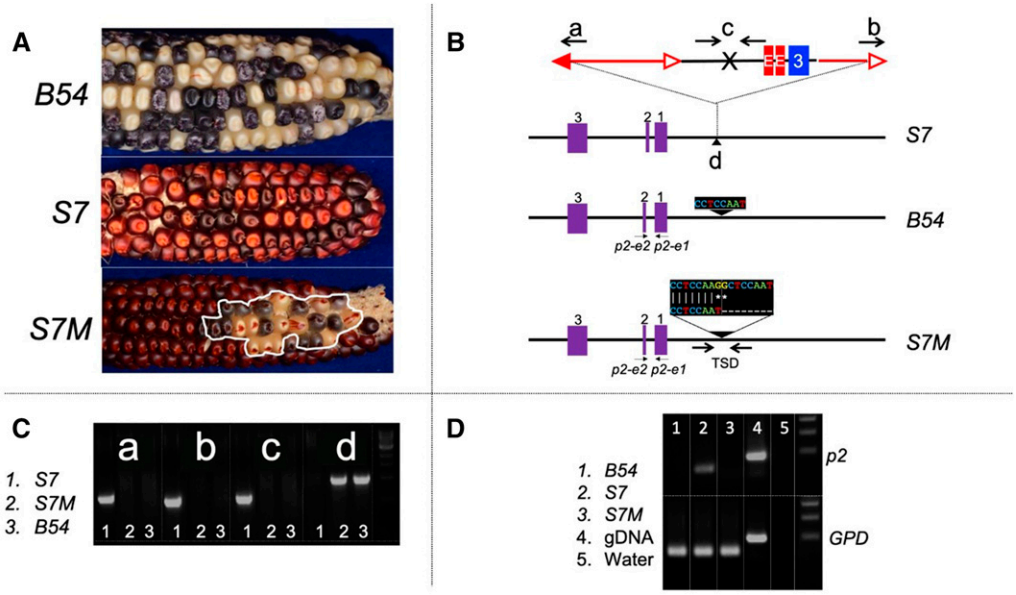

Figure 6 Isolation and analysis of CI-excision allele *p2-S7M*. (A) Phenotypes of *p1-wwB54*, *p2-S7*, and *p2-S7M* origin ear. *P2-S7M* origin ear has predominantly red pericarp conditioned by *p2-S7* and a large multikernel sector (outlined in white) from which the *S7M* allele was obtained. Note that the intensity of red kernel pericarp pigmentation can vary among ears due to genetic background and field conditions. (B) Structures of *S7*, *B54*, and *S7M*. Letters and arrows indicate CI features analyzed by PCR; sequences indicate the target site in *B54*, and the TSD in *S7M*; arrows labeled p2-e1 and p2-e2 indicate the primers used in RT-PCR. (C) PCR analysis of CI features in *S7*, *S7M*, and *B54*; a–d indicate corresponding features in *S7* (Figure 6B). (D) RT-PCR results showing the presence of *p2* transcripts in *S7*, and absence in *B54* and *S7M*. Lane 4 (gDNA) is a control containing *S7M* gDNA as template. The larger-sized products in gDNA lanes result from PCR across introns in *p2* and *GPD* genes. CI, composite insertion; gDNA, genomic DNA; TSD, target site duplication.

P2-CI epiallele has altered DNA methylation

As noted above, some *p2-CI* alleles exhibited sectors and progeny ears with reduced pericarp pigment intensity. One case analyzed was derived from the *p2-CI-E3* allele, which contains a 15.9-kb CI inserted in the 5′ region of *p2*. This variant (termed *E3M*) was isolated from a single kernel in a small sector of light orange pericarp on an otherwise red *E3* ear (Figure 7A). Progeny plants grown from this kernel have distinctly lighter orange kernel pericarp, indicating a heritable reduction in *p2* expression in *E3M*. However, unlike the CI-excision allele *S7M*, PCR analysis of the *Ac*, *fAc*, and internal junctions showed that *E3M* does not have any structural variations in the CI target site (Figure 7, B and C). We hypothesized that the *E3M* dilute-pigment phenotype was caused by epigenetic change(s) rather than structural variation. Epigenetic variations such as DNA methylation are known to be correlated with changes in gene expression (Assaad *et al.* 1993). Therefore, we conducted bisulfite sequencing of seven targeted regions in *p1* and *p2* to analyze DNA methylation at single-base resolution (File S8). We examined methylation of the *f15* enhancer fragment, *Ac* and *fAc* junctions in the *p1* background, and the CIs of *E3* and *E3M*, as well as the *p2* sequences flanking both *Ac-CI* and *fAc-CI* (File S9 and File S10). The results showed that in the tested enhancer fragment and the *p2* flanking sequences, cytosines are unmethylated and there is no detectable difference between *B54*, *E3*, and *E3M* (File S9 and File S10). In contrast, some methylation changes were observed in *Ac* and *fAc* sequences. In the first 100 bp of the *Ac* 5′ end, there are 23 cytosines. In the background *Ac*, *B54* has four methylated cytosines in this region; while *E3* and *E3M* have 12 and 9 methylated cytosines, respectively (File S9 and File S10). In the CI *Ac*, *E3* has a net +1 additional methylated cytosine compared to the background *Ac*; this results from one demethylation and two *de novo* methylations. In *E3M*, the CI *Ac* has three *de novo* methylated cytosines compared to the background *Ac*. In the first 100 bp of the *fAc* 3′ end, there are 18 cytosine residues; in the background *fAc*, *B54* has 10 methylated cytosines in this region, while *E3* and *E3M* have 10 and 12 methylated residues, respectively. In the CI *fAc*, *E3* has the same methylation pattern as the background, while *E3M* has one demethylated cytosine and one *de novo* methylation (File S9 and File S10). These results showed that methylation does not change dramatically between the *E3* and *E3M* alleles in the *Ac* and *fAc* segments analyzed. However, a recent report indicates that changes in methylation at a single CpG can influence transcription factor binding (Yang *et al.* 2020). Although methylation of *Ac* sequences is known to affect *Ac* transcription (Kunze *et al.* 1988), further work will be required to determine whether the observed differences in methylation of *E3* and *E3M* are causally associated with differential expression of *p2*.

Discussion

TEs are usually considered to be selfish DNA providing little or no benefit to the host genome (Orgel *et al.* 1980). Many studies have shown that TEs often have deleterious effects such as disrupting gene structures and modifying the

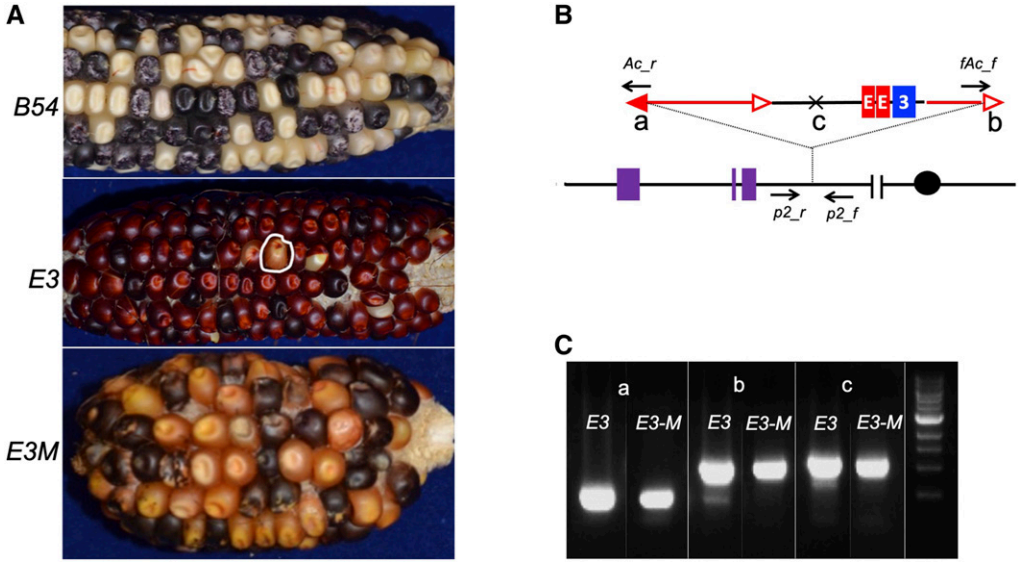

Figure 7 Epiallele *E3M* derived from CI *E3*. (A) Ear and kernel pericarp phenotypes of *B54*, *E3*, and *E3M*. Epiallele *E3M* originated from pale kernel outlined in *E3*. (B) Structure of *CI-E3* allele showing locations of PCR primers used to confirm *E3* and *E3M* CI insertions. (C) PCR results of *Ac*, *fAc*, and the internal junctions corresponding to 7B (A–C). CI, composite insertion; *fAc*, fractured *Ac*.

epigenetic features near their insertion sites (Hollister and Gaut 2009; Zuo *et al.* 2016). However, recent reports have shown that TEs can modify coding sequences and regulate gene expression to potentially increase the fitness of the host (Chuong *et al.* 2017). For example, TEs can perform enhancer-like functions in eukaryotic genomes. In the human genome, widespread enhancers overlap with TEs (Cao *et al.* 2019), and experimental data have confirmed that a subset of TE enhancers play important roles in gene regulation in early mouse development (Todd *et al.* 2019). These studies support the idea that TE domestication is important in eukaryotic genome evolution; however, most of these reports were focused on class I TEs in animal and human systems (Sundaram and Wysocka 2020). In this study, we identify a new mechanism by which class II TEs can regulate genes in maize. We demonstrate that, in addition to evolving into regulatory elements over time, TEs can induce sudden changes in gene expression by acquiring and mobilizing existing genomic enhancer elements.

In previous studies, we have described the mechanism of RET-induced DNA rereplication in maize (Zhang *et al.* 2014). This rereplication process is initiated by *Ac/fAc* transposition, which generates a rolling circle replicon to replicate the TE and flanking sequences during an additional round in the same cell cycle. This can produce a CI at the *Ac/fAc* insertion site. Here we show that, during their formation, CIs can acquire a regulatory element, enhancer *f15* of the *p1* gene, and activate expression of the *p2* gene, which is normally not expressed in kernel pericarp. By screening maize ears from plants of genotype *p1-wwB54*, which contains reverse-orientated *Ac/fAc* termini, we obtained a series of red pericarp alleles containing CIs inserted in or near the *p2* gene: among 24 mapped CIs, 10 were inserted in the upstream sequences of *p2*, while 14 inserted in *p2* intron 2. CI insertions upstream of *p2* can induce transcription of the intact *p2* gene; while CI insertion into *p2* intron 2 can generate a chimeric *p2/p1* gene (Zhang and Peterson 2005; Wang *et al.* 2015). A few insertion hotspots were observed: five CIs inserted into a <200-bp region upstream of *p2* (positions −3188 to −3364) and four CIs inserted into a <100-bp region in *p2* intron 2 (positions 8017–8102). Moreover, some CIs insert very closely to each other, or even at the same site (L12 and S7; TZ3-1 and TZ3-12; and S10 and TZ3-17). We did not detect any clear sequence signatures in these hotspots (Vollbrecht *et al.* 2010) (data not shown); it is possible that insertion site preference is influenced by epigenetic modifications.

We analyzed the detailed structures of 10 CIs ranging in size from 12.8 to 23.6 kb. All were composed of *Ac* and *fAc* elements enclosing duplications of *p1* sequences flanking the original donor elements. These duplications were joined together at internal junctions with sequences characteristic of fusion by NHEJ, accompanied by the presence of filler DNA sequences in one-half of the cases. These structures are all consistent with a model of CI formation by DNA rereplication induced by RET (Zhang *et al.* 2014). Notably, all the CIs included copies of enhancer fragment *f15* derived from the *p1* gene 3′ region.

Activation of *p2* expression by the enhancer-containing CI was confirmed by analysis of a particular case, *S7M*, in which the complete CI excised as a macrotransposon. CI excision resulted in heritable loss of kernel pericarp pigmentation and elimination of *p2* RNA, proving that the red pericarp phenotype was caused by CI-induced *p2* expression. Another variant allele (*E3M*), which specified orange pericarp phenotype, was analyzed and found to have some DNA methylation changes in the terminal sequences of the CI *Ac* and *fAc* elements. Although it is not clear whether these methylation differences are responsible for the differences in *p2* expression, it is known that TE DNA methylation can impact the expression of nearby genes (Wittmeyer *et al.* 2018).

RET is one type of alternative transposition, a transposition mechanism involving the termini of two different TEs (Gray

2000). A second type of alternative transposition is termed SCT, in which the two TEs are located on sister chromatids (Weil and Wessler 1993; Zhang and Peterson 1999). Recently, SCT has been shown to generate CIs containing inverted duplications of TE sequences that can induce silencing of *Ac* (Wang *et al.* 2020). Together, these results indicate that alternative transpositions are able to copy and mobilize regulatory elements and thereby regulate gene expression patterns, while other alternative transposition events can initiate TE silencing. These mechanisms are meaningful in plant development and genome evolution. Depending on the length of the rereplication, CIs enlarge the genome by various sizes. Furthermore, the target *p1/p2* locus plays a central role in regulating phlobaphene biosynthesis in maize tissues (Grotewold *et al.* 1994). Because phlobaphene pigment accumulation is correlated with kernel pericarp thickness and reduced mycotoxin contamination on maize kernels (Landoni *et al.* 2020), the ectopic expression of *p2* induced by CI alleles could be beneficial.

Although TEs proliferate and contribute to a large portion of repetitive sequences in the evolutionary process, most TEs are epigenetically silenced and heavily methylated in both plant and animal genomes (Aravin and Bourc'his 2008; Hollister and Gaut 2009; Panda *et al.* 2016). Moreover, the silencing signal can spread beyond the TE and affect the flanking sequence and nearby genes (Noshay *et al.* 2019). These silenced TEs are immobile or reduced in transposition potential, and thus are hardly able to generate large genome rearrangements. In maize, *Mu* and *Ac/Ds* elements have been characterized as active TE families that tend to land in low-methylation regions with open chromatin structures (Springer *et al.* 2018). In this study, we show that after CIs insert to the target sites, the *Ac* element is still active and can induce transposition of itself and nonautonomous *Ds* elements. Furthermore, the *S7M* mutant derived from the *S7* allele indicates that the complete CI can move as a macrotransposon. Although we did not detect reinsertion of the S7 CI, it is quite possible that a macrotransposon of this size (17.2 kb) can excise and reinsert in the genome (Huang and Dooner 2008). Mutation or loss of the CI *Ac* 3′ end would prevent independent excision of the *Ac* element, converting the complex CI macrotransposon into a single mobile element. This provides one plausible mechanism for sequence acquisition by TIR elements. For CIs that contain functional enhancers as described here, such cases may be considered as authentic controlling elements, as originally described by McClintock (1956).

In this study, we used *Ac/fAc* and the *p1/p2* loci as examples to reveal the potential regulatory role of alternative transpositions in genome evolution. Because our screen was based on the recovery of pericarp pigment, we detected only CI insertions into the *p2* locus. In fact, CIs can insert into any location in the genome (Zhang *et al.* 2014; Wang *et al.* 2020), not necessarily producing a readily observable phenotype. The occurrence of a pair of active TEs (*Ac/fAc)* inserted into one copy of closely linked paralogs (*p1/p2)* controlling a visible, nonessential trait provides an ideal system in which to detect such events in real time, in relatively small experimental populations. It may be argued that similar haplotypes are so rare in natural stocks that their true impact is very small. However, because maize genomes contain >50,000 full-length TIR TEs (Su *et al.* 2019), as well as many more copies of partial and fractured elements (Su *et al.* 2020), RET events involving some TE systems and affecting a variety of genes may have occurred frequently over evolutionary time. Alternative transpositions have also been identified in snapdragon *Tam3* elements (Martin and Lister 1989) and *Drosophila P* elements (Gray *et al.* 1996), suggesting that this mechanism could potentially be an important source of regulatory modification in both plant and animal genomes.

Acknowledgments

We thank Terry Olson for technical assistance, and Jianbo Zhang and Dafang Wang for suggestions on the experiments. This research is supported by the USDA National Institute of Food and Agriculture Hatch project number IOW05282, and by State of Iowa funds.

Author contributions: W.S., T.Z., and T.P. conceived and designed the experiment; W.S. and T.Z. performed the experiments; and W.S. and T.P. wrote the paper.

Literature Cited

Anderson, E. G., 1924 Pericarp studies in maize. II. The allelomorphism of a series of factors for pericarp color. Genetics 9: 442–453.

Aravin, A. A., and D. Bourc'his, 2008 Small RNA guides for de novo DNA methylation in mammalian germ cells. Genes Dev. 22: 970–975. https://doi.org/10.1101/gad.1669408

Assaad, F. F., K. L. Tucker, and E. R. Signer, 1993 Epigenetic repeat-induced gene silencing (RIGS) in Arabidopsis. Plant Mol. Biol. 22: 1067–1085. https://doi.org/10.1007/BF00028978

Blackwood, E. M., and J. T. Kadonaga, 1998 Going the distance: a current view of enhancer action. Science 281: 60–63. https://doi.org/10.1126/science.281.5373.60

Butelli, E., C. Licciardello, Y. Zhang, J. Liu, S. Mackay *et al.*, 2012 Retrotransposons control fruit-specific, cold-dependent accumulation of anthocyanins in blood oranges. Plant Cell 24: 1242–1255. https://doi.org/10.1105/tpc.111.095232

Cao, Y., G. Chen, G. Wu, X. Zhang, J. McDermott *et al.*, 2019 Widespread roles of enhancer-like transposable elements in cell identity and long-range genomic interactions. Genome Res. 29: 40–52. https://doi.org/10.1101/gr.235747.118

Chalmers, R. M., and N. Kleckner, 1996 IS10/Tn10 transposition efficiently accommodates diverse transposon end configurations. EMBO J. 15: 5112–5122. https://doi.org/10.1002/j.1460-2075.1996.tb00892.x

Chuong, E. B., N. C. Elde, and C. Feschotte, 2017 Regulatory activities of transposable elements: from conflicts to benefits. Nat. Rev. Genet. 18: 71–86. https://doi.org/10.1038/nrg.2016.139

Clark, R. M., T. N. Wagler, P. Quijada, and J. Doebley, 2006 A distant upstream enhancer at the maize domestication gene tb1 has pleiotropic effects on plant and inflorescent architecture. Nat. Genet. 38: 594–597. https://doi.org/10.1038/ng1784

Doebley, J., A. Stec, and C. Gustus, 1995 Teosinte branched1 and the origin of maize: evidence for epistasis and the evolution of dominance. Genetics 141: 333–346.

Dooner, H. K., T. P. Robbins, and R. A. Jorgensen, 1991 Genetic and developmental control of anthocyanin biosynthesis. Annu. Rev. Genet. 25: 173–199. https://doi.org/10.1146/annurev.ge.25.120191.001133

Eichten, S. R., N. A. Ellis, I. Makarevitch, C. T. Yeh, J. I. Gent *et al*., 2012 Spreading of heterochromatin is limited to specific families of maize retrotransposons. PLoS Genet. 8: e1003127. https://doi.org/10.1371/journal.pgen.1003127

Emerson, R. A., 1917 Genetical studies of variegated pericarp in maize. Genetics 2: 1–35.

Emerson, R. A., 1929 The frequency of somatic mutation in variegated pericarp of maize. Genetics 14: 488–511.

Gray, Y. H., 2000 It takes two transposons to tango: transposable-element-mediated chromosomal rearrangements. Trends Genet. 16: 461–468. https://doi.org/10.1016/S0168-9525(00)02104-1

Gray, Y. H., M. M. Tanaka, and J. A. Sved, 1996 P-element-induced recombination in Drosophila melanogaster: hybrid element insertion. Genetics 144: 1601–1610.

Grotewold, E., P. Athma, and T. Peterson, 1991 Alternatively spliced products of the maize P gene encode proteins with homology to the DNA-binding domain of myb-like transcription factors. Proc. Natl. Acad. Sci. USA 88: 4587–4591. https://doi.org/10.1073/pnas.88.11.4587

Grotewold, E., B. J. Drummond, B. Bowen, and T. Peterson, 1994 The myb-homologous P gene controls phlobaphene pigmentation in maize floral organs by directly activating a flavonoid biosynthetic gene subset. Cell 76: 543–553. https://doi.org/10.1016/0092-8674(94)90117-1

Hirsch, C. D., and N. M. Springer, 2017 Transposable element influences on gene expression in plants. Biochim. Biophys. Acta. Gene Regul. Mech. 1860: 157–165. https://doi.org/10.1016/j.bbagrm.2016.05.010

Hollister, J. D., and B. S. Gaut, 2009 Epigenetic silencing of transposable elements: a trade-off between reduced transposition and deleterious effects on neighboring gene expression. Genome Res. 19: 1419–1428. https://doi.org/10.1101/gr.091678.109

Huang, J. T., and H. K. Dooner, 2008 Macrotransposition and other complex chromosomal restructuring in maize by closely linked transposons in direct orientation. Plant Cell 20: 2019–2032. https://doi.org/10.1105/tpc.108.060582

Krivega, I., and A. Dean, 2012 Enhancer and promoter interactions-long distance calls. Curr. Opin. Genet. Dev. 22: 79–85. https://doi.org/10.1016/j.gde.2011.11.001

Kunze, R., P. Starlinger, and D. Schwartz, 1988 DNA methylation of the maize transposable element Ac interferes with its transcription. Mol. Gen. Genet, 214: 325–327. https://doi.org/10.1007/BF00337730

Landoni, M., D. Puglisi, E. Cassani, G. Borlini, G. Brunoldi *et al*., 2020 Phlobaphenes modify pericarp thickness in maize and accumulation of the fumonisin mycotoxins. Sci. Rep. 10: 1417. https://doi.org/10.1038/s41598-020-58341-8

Lechelt, C., T. Peterson, A. Laird, J. Chen, S. L. Dellaporta *et al*., 1989 Isolation and molecular analysis of the maize P locus. Mol. Gen. Genet. 219: 225–234. https://doi.org/10.1007/BF00261181

Li, L.-C., and R. Dahiya, 2002 MethPrimer: designing primers for methylation PCRs. Bioinformatics 18: 1427–1431. https://doi.org/10.1093/bioinformatics/18.11.1427

Luehrsen, K. R., and V. Walbot, 1990 Insertion of Mu1 elements in the first intron of the Adh1-S gene of maize results in novel RNA processing events. Plant Cell 2: 1225–1238.

Makarevitch, I., A. J. Waters, P. T. West, M. Stitzer, C. N. Hirsch *et al*., 2015 Transposable elements contribute to activation of maize genes in response to abiotic stress. PLoS Genet. 11: e1004915 (erratum: PLoS Genet. 11: e1005566). https://doi.org/10.1371/journal.pgen.1004915

Martin, C., and C. Lister, 1989 Genome juggling by transposons: Tam3-induced rearrangements in Antirrhinum majus. Dev. Genet. 10: 438–451. https://doi.org/10.1002/dvg.1020100605

McClintock, B., 1947 Mutable loci in maize, pp. 155–169 in *Annual Report of the Director of the Department of Genetics, Carnegie Institution of Washington Year Book No. 47, 1947-1948*, Carnegie Institution of Washington, Cold Spring Harbor, NY.

McClintock, B., 1950 The origin and behavior of mutable loci in maize. Proc. Natl. Acad. Sci. USA 36: 344–355. https://doi.org/10.1073/pnas.36.6.344

McClintock, B., 1956 Controlling elements and the gene. *Cold Spring Harb. Symp. Quant. Biol*. **21:** 197–216.

McVey, M., and S. E. Lee, 2008 MMEJ repair of double-strand breaks (director's cut): deleted sequences and alternative endings. Trends Genet. 24: 529–538. https://doi.org/10.1016/j.tig.2008.08.007

Moore, J. K., and J. E. Haber, 1996 Cell cycle and genetic requirements of two pathways of nonhomologous end-joining repair of double-strand breaks in Saccharomyces cerevisiae. Mol. Cell. Biol. 16: 2164–2173. https://doi.org/10.1128/MCB.16.5.2164

Noshay, J. M., S. N. Anderson, P. Zhou, L. Ji, W. Ricci *et al*., 2019 Monitoring the interplay between transposable element families and DNA methylation in maize. PLoS Genet. 15: e1008291. https://doi.org/10.1371/journal.pgen.1008291

Oka, R., J. Zicola, B. Weber, S. N. Anderson, C. Hodgman *et al*., 2017 Genome-wide mapping of transcriptional enhancer candidates using DNA and chromatin features in maize. Genome Biol. 18: 137. https://doi.org/10.1186/s13059-017-1273-4

Orgel, L. E., F. Crick, and C. Sapienza, 1980 Selfish DNA. Nature 288: 645–646. https://doi.org/10.1038/288645a0

Panda, K., L. Ji, D. A. Neumann, J. Daron, R. J. Schmitz *et al*., 2016 Full-length autonomous transposable elements are preferentially targeted by expression-dependent forms of RNA-directed DNA methylation. Genome Biol. 17: 170. https://doi.org/10.1186/s13059-016-1032-y

Peterson, T., and J. Zhang, 2013 *The mechanism of Ac/Ds transposition*, pp. 41–59 in Plant Transposons and Genome Dynamics in Evolution, edited by N. V. Fedoroff. Wiley-Blackwell, Hoboken, NJ.

Sidorenko, L., X. Li, L. Tagliani, B. Bowen, and T. Peterson, 1999 Characterization of the regulatory elements of the maize P-rr gene by transient expression assays. Plant Mol. Biol. 39: 11–19. https://doi.org/10.1023/A:1006172815663

Springer, N. M., S. N. Anderson, C. M. Andorf, K. R. Ahern, F. Bai *et al*., 2018 The maize W22 genome provides a foundation for functional genomics and transposon biology. Nat. Genet. 50: 1282–1288. https://doi.org/10.1038/s41588-018-0158-0

Stam, M., C. Belele, J. E. Dorweiler, and V. L. Chandler, 2002 Differential chromatin structure within a tandem array 100 kb upstream of the maize b1 locus is associated with paramutation. Genes Dev. 16: 1906–1918. https://doi.org/10.1101/gad.1006702

Su, W., X. Gu, and T. Peterson, 2019 TIR-Learner, a new ensemble method for TIR transposable element annotation, provides evidence for abundant new transposable elements in the maize genome. Mol. Plant 12: 447–460. https://doi.org/10.1016/j.molp.2019.02.008

Su, W., S. Ou, M. B. Hufford, and T. Peterson, 2020 A tutorial of EDTA: extensive *de-novo* TE Annotator. Methods Mol. Biol. 2250 (in press).

Sundaram, V., and J. Wysocka, 2020 Transposable elements as a potent source of diverse cis-regulatory sequences in mammalian genomes. Philos. Trans. R. Soc. Lond. B Biol. Sci. 375: 20190347. https://doi.org/10.1098/rstb.2019.0347

Todd, C. D., Ö. Deniz, D. Taylor, and M. R. Branco, 2019 Functional evaluation of transposable elements as enhancers in mouse embryonic and trophoblast stem cells. Elife 8: e44344. https://doi.org/10.7554/eLife.44344

Vollbrecht, E., J. Duvick, J. P. Schares, K. R. Ahern, P. Deewatthanawong *et al.*, 2010 Genome-wide distribution of transposed Dissociation elements in maize. Plant Cell 22: 1667–1685. https://doi.org/10.1105/tpc.109.073452

Wang, D., C. Yu, T. Zuo, J. Zhang, D. F. Weber *et al.*, 2015 Alternative transposition generates new chimeric genes and segmental duplications at the maize p1 locus. Genetics 201: 925–935. https://doi.org/10.1534/genetics.115.178210

Wang, D., J. Zhang, T. Zuo, M. Zhao, D. Lisch *et al.*, 2020 Small RNA-mediated de novo silencing of Ac/ds transposons is initiated by alternative transposition in maize. Genetics 215: 393–406. https://doi.org/10.1534/genetics.120.303264

Weil, C. F., and S. R. Wessler, 1993 Molecular evidence that chromosome breakage by Ds elements is caused by aberrant transposition. Plant Cell 5: 515–522. https://doi.org/10.1105/tpc.5.5.515

Wessler, S., A. Tarpley, M. Purugganan, M. Spell, and R. Okagaki, 1990 Filler DNA is associated with spontaneous deletions in maize. Proc. Natl. Acad. Sci. USA 87: 8731–8735. https://doi.org/10.1073/pnas.87.22.8731

Wicker, T., F. Sabot, A. Hua-Van, J. L. Bennetzen, P. Capy *et al.*, 2007 A unified classification system for eukaryotic transposable elements. Nat. Rev. Genet. 8: 973–982. https://doi.org/10.1038/nrg2165

Wittmeyer, K., J. Cui, D. Chatterjee, T. F. Lee, Q. Tan *et al.*, 2018 The dominant and poorly penetrant phenotypes of maize unstable factor for orange1 are caused by DNA methylation changes at a linked transposon. Plant Cell 30: 3006–3023. https://doi.org/10.1105/tpc.18.00546

Yang, L., Z. Chen, E. S. Stout, F. Delerue, L. M. Ittner *et al.*, 2020 Methylation of a CGATA element inhibits binding and regulation by GATA-1. Nat. Commun. 11: 1–10.

Yu, C., J. Zhang, V. Pulletikurti, D. F. Weber, and T. Peterson, 2010 Spatial configuration of transposable element Ac termini affects their ability to induce chromosomal breakage in maize. Plant Cell 22: 744–754. https://doi.org/10.1105/tpc.109.070052

Yu, C., J. Zhang, and T. Peterson, 2011 Genome rearrangements in maize induced by alternative transposition of reversed Ac/Ds termini. Genetics 188: 59–67. https://doi.org/10.1534/genetics.111.126847

Zhang, J., and T. Peterson, 1999 Genome rearrangements by nonlinear transposons in maize. Genetics 153: 1403–1410.

Zhang, J., and T. Peterson, 2004 Transposition of reversed Ac element ends generates chromosome rearrangements in maize. Genetics 167: 1929–1937. https://doi.org/10.1534/genetics.103.026229

Zhang, J., and T. Peterson, 2005 A segmental deletion series generated by sister-chromatid transposition of Ac transposable elements in maize. Genetics 171: 333–344. https://doi.org/10.1534/genetics.104.035576

Zhang, P., S. Chopra, and T. Peterson, 2000 A segmental gene duplication generated differentially expressed myb-homologous genes in maize. Plant Cell 12: 2311–2322. https://doi.org/10.1105/tpc.12.12.2311

Zhang, J., F. Zhang, and T. Peterson, 2006 Transposition of reversed Ac element ends generates novel chimeric genes in maize. PLoS Genet. 2: e164. https://doi.org/10.1371/journal.pgen.0020164

Zhang, J., C. Yu, V. Pulletikurti, J. Lamb, T. Danilova *et al.*, 2009 Alternative Ac/Ds transposition induces major chromosomal rearrangements in maize. Genes Dev. 23: 755–765. https://doi.org/10.1101/gad.1776909

Zhang, J., T. Zuo, and T. Peterson, 2013 Generation of tandem direct duplications by reversed-ends transposition of maize Ac elements. PLoS Genet. 9: e1003691. https://doi.org/10.1371/journal.pgen.1003691

Zhang, J., T. Zuo, D. Wang, and T. Peterson, 2014 Transposition-mediated DNA re-replication in maize. Elife 3: e03724. https://doi.org/10.7554/eLife.03724

Zuo, T., J. Zhang, A. Lithio, S. Dash, D. F. Weber *et al.*, 2016 Genes and small RNA transcripts exhibit dosage-dependent expression pattern in maize copy-number alterations. Genetics 203: 1133–1147. https://doi.org/10.1534/genetics.116.188235

Communicating editor: J. Birchler